Three-dimensional flow prediction in mould filling processes using a GFDM

Felix R. Saucedo-Zendejo, Edgar O. Reséndiz-Flores & Jörg Kuhnert

Computational Particle Mechanics

ISSN 2196-4378

Comp. Part. Mech.
DOI 10.1007/s40571-019-00222-7

Springer

Computational Particle Mechanics
https://doi.org/10.1007/s40571-019-00222-7

Three-dimensional flow prediction in mould filling processes using a GFDM

Felix R. Saucedo-Zendejo[1] · Edgar O. Reséndiz-Flores[1] · Jörg Kuhnert[2]

Received: 10 July 2018 / Revised: 30 December 2018 / Accepted: 2 January 2019

Abstract
The aim of this work is to achieve a meshfree implementation for the numerical prediction of 3D flows during mould filling processes in metal casting using a generalized finite difference method. The free surface incompressible flow problem is numerically solved using a semi-implicit Chorin–Uzawa's projection scheme where the normal vectors needed for the free surface computations are computed with a simple and efficient idea. Further, the boundary conditions incorporation involved in this industrial problem is done in a simple and direct manner. The main characteristics in this meshfree formulation together with details of its computational implementation are given. The numerical results of a benchmark example using this formulation are reported and compared with published numerical and experimental results, and finally, the numerical solution of some three-dimensional test problems is reported which show that this formulation is promising for predicting three-dimensional complex free surface flows in mould filling processes in casting.

Keywords Casting · Generalized finite difference method · FPM · Free surface flow · Meshless method · Finite pointset method

1 Introduction

Many industrial applications require the production of components with precise shapes and/or dimensions, which could be very complex. Metal casting techniques are one of the most widely used procedures to achieve this purpose. Such processes begin with a step in which a mould's cavity is filled with molten material followed by a step of complete solidification inside the mould [29]. The mould filling step is very important because the final structural characteristics and the number of defects in the manufactured components are determined through it. It involves a free surface flow with high geometric complexity, which can be divided into jets or sprayed inside the mould during the filling. Therefore, a set of defects in the manufactured products could be originated during this filling step which are principally due to the additional free surfaces formation which leads to the generation of secondary phase layers, as, for example, oxide layers when the casting procedure occurs in a nominal atmosphere [5].

Numerical modelling is frequently used to understand and improve rapidly changing and flows with free surfaces as those arising in mould filling processes since it provides a huge amount of valuable information which is tough to obtain with other kinds of procedures [15]. These numerical simulations are usually based on classical mesh-based methods such as finite volume method (FVM) [2], finite element method (FEM) [19,23,25] and finite difference method (FDM) [16,22], and commonly they use the level-set method (LSM), volume-of-fluid method (VOF) or marker-and-cell method (MAC) to track free surfaces [15,33]. Nevertheless, mesh-based methods require the use of remeshing approaches in order to simulate problems involving free surface flows, which lead to solutions with degraded accuracy and are computationally expensive. This drawback arises from the requirement of using a predefined element mesh to solve the governing equations [3,20].

Meshless or meshfree methods have been developed in recent decades as an alternative to the classical mesh-based techniques since they let to overcome some of the drawbacks in such methods [3,20,24]. One of the first meshfree methods

✉ Felix R. Saucedo-Zendejo
feliks@live.com.mx

[1] Division of Postgraduate Studies and Research, The Technological Institute of Saltillo, National Institute of Technology of Mexico, Blvd. V. Carranza 2400, Col. Tecnológico, C.P. 25280 Saltillo, Coahuila, Mexico

[2] Fraunhofer-Institut für Techno-und Wirtschaftsmathematik, Fraunhofer-Platz-1, 67663 Kaiserslautern, Germany

Published online: 08 January 2019

that were developed is the so smoothed particle hydrodynamics (SPH), which is the most widely established Lagrangian method [36,37]. This method has shown to be very useful in predicting complex free surface flows, and it is able to tolerate large deformations, sprays and domain fragmentation. Due to these features, it has been applied in injection moulding, metal forming, extrusion and mould filling in casting processes [1,4,6–10,21]. Nevertheless, since the development of its first version, it suffered inconsistency, instability and difficulties in the boundary conditions incorporation so that over the years, a lot of improvements and enhancements were incorporated to the original SPH formulation [20,24] and many alternative meshfree methods have been proposed [11–13,17,27,28,38].

A truly meshless generalized finite difference method (GFDM) which is able to overcome many of the constraints found in SPH, particularly those related with the boundary conditions incorporation, is the so-called finite pointset method (FPM) proposed by Kuhnert [18]. This meshfree method has shown to be far superior to the common mesh-based and some other meshfree techniques for the modelling of fluid dynamics problems involving free surfaces, rapidly changing domains or multiphase flows [14,34,40–42]. FPM is a Lagrangian strong-form method which uses the weighted least-squares (WLSM) interpolation method to solve general elliptic partial differential equations and for computing spatial derivatives [42]. Some of the advantages of this meshfree method are its comparably simple computational implementation and that the boundary conditions are implemented in a natural way just prescribing them on those particles located on boundaries [40].

This makes FPM very attractive to simulate mould filling processes in casting where very complex geometries, free surface flows and rapidly changing domains are present. The classical FPM formulation has shown to be feasible and suitable for the numerical simulation of free surface flows in mould filling processes [32]. Nevertheless, its explicit formulation makes its potential limited in some practical applications. Consequently, it is natural to try to use implicit or semi-implicit formulations which let to use larger time step sizes and numerical schemes with higher order of accuracy. The semi-implicit FPM formulation proposed in Saucedo-Zendejo and Reséndiz-Flores [34] is considered an enhancement on the classical FPM approach since it allows an implicit and coupled computation of the field variables, and it was specially developed to deal with free surface flows. Therefore, with the aim of developing a robust simulation software for industrial mould filling processes in casting, in this work we propose the application of the semi-implicit FPM formulation [34] for the numerical prediction of three-dimensional mould filling processes. In order to get some insight into its performance, the numerical solution of some benchmark examples using this approach is reported which show that it is a promising tool for the prediction of 3D free surface flows in casting mould filling processes. Moreover, this is the first time that this semi-implicit FPM formulation is applied and tested for mould filling processes simulation and that the three-dimensional numerical results for the proposed examples using this meshfree formulation are reported in the literature.

The structure of this paper is as follows: Sect. 2 introduces the governing equations for free surface flows and the numerical scheme for the solution of the corresponding differential equations. Section 3 describes the FPM basic ideas and the semi-implicit formulation to solve the free surface flow problem in mould filling. Section 4 deals with some implementation aspects. The numerical simulation of several test problems using this formulation is presented in Sect. 5 followed by the conclusions in the last section.

2 Mathematical model

The mathematical model for free surface incompressible flows during mould filling processes in metal casting is the Lagrangian incompressible Navier–Stokes equations

$$\frac{D\mathbf{v}}{Dt} = -\frac{1}{\rho}\nabla p + \nu\nabla^2\mathbf{v} + \mathbf{f}, \tag{1}$$

$$\nabla \cdot \mathbf{v} = 0, \tag{2}$$

where ν is the kinematic viscosity, p is the pressure, ρ is the density, $\mathbf{v}$ is the velocity and $\mathbf{f}$ is the acceleration vector due to all the body forces. These equations are completed with the following set of boundary and initial conditions

$$\mathbf{v}|_{t=0} = \mathbf{v}_0, \tag{3}$$

$$\mathbf{v}|_{\partial\Omega_1} = \mathbf{0}, \tag{4}$$

$$\mathbf{v}\cdot\mathbf{n}|_{\partial\Omega_2} = 0, \tag{5}$$

$$\left.\frac{\partial\,(\mathbf{v}\cdot\mathbf{t}_i)}{\partial\mathbf{n}}\right|_{\partial\Omega_2} = 0, \tag{6}$$

$$(\tau - \mathbf{I}p)\,\mathbf{n}|_{\partial\Omega_3} = \sigma\kappa\mathbf{n}, \tag{7}$$

$$\left.\mathbf{t}_i^{\mathrm{T}}\tau\mathbf{n}\right|_{\partial\Omega_3} = 0, \tag{8}$$

where $\partial\Omega_1$ is a no-slip solid wall boundary condition, $\partial\Omega_2$ is a free-slip solid wall boundary condition, $\partial\Omega_3$ is a free surface boundary condition, τ is the viscous stress tensor, κ is the curvature on the free surface, σ is the surface tension, $\mathbf{n}$ is an outward orthonormal vector, $\mathbf{t}_i$ is a tangential unitary vector to the boundary, for $i = 1, 2$, and $\mathbf{v}_0$ is the initial velocity on Ω.

In order to solve Eqs. (1) and (2) with the initial and boundary conditions (3)–(8) in a simple and natural way, a semi-implicit Chorin–Uzawa's projection formulation of

first order of accuracy will be used [26]. Now, let $\mathbf{r}$ to be a set of particles discretizing the fluid and distributed on the whole domain and its boundaries. Such particles carry all the field variables such as velocities and pressures. Let $\mathbf{r}^n$ and $\mathbf{v}^n$ be initially given. They denote the particles location and its velocities at time t^n, respectively. The semi-implicit Chorin–Uzawa's projection formulation consists of the following steps [34]:

1. Explicitly update the particles positions through

$$\mathbf{r}^{n+1} = \mathbf{r}^n + \Delta t \mathbf{v}^n. \tag{9}$$

2. Implicitly compute the intermediate velocities

$$\mathbf{v}^* - \Delta t \nu \nabla^2 \mathbf{v}^* = \mathbf{v}^n + \Delta t \mathbf{f}^{n+1}, \tag{10}$$

with the boundary and initial conditions (3)–(8).

3. Implicitly compute the artificial pressure

$$\nabla \varphi = \frac{\rho}{\Delta t} \nabla \cdot \mathbf{v}^*, \tag{11}$$

with the following boundary conditions

$$\left.\frac{\partial \varphi}{\partial \mathbf{n}}\right|_{\partial\Omega_1, \partial\Omega_2} = 0, \tag{12}$$

$$\varphi|_{\partial\Omega_3} = 0. \tag{13}$$

4. Update/correct the intermediate velocity

$$\mathbf{v}^{n+1} = \mathbf{v}^* - \frac{\Delta t}{\rho} \nabla \varphi \tag{14}$$

5. Update/correct the pressure field

$$p^{n+1} = \varphi - \rho \nu \nabla \cdot \mathbf{v}^*. \tag{15}$$

3 The finite pointset method (FPM)

In this section, the main FPM ideas proposed by Kuhnert [18] are described. Following [40]:

Let Ω be a given domain with boundary $\partial\Omega$ and suppose that a set of particles $\mathbf{r}_1, \mathbf{r}_2, \ldots, \mathbf{r}_N$ are distributed in the domain with corresponding function values $f(\mathbf{r}_1), f(\mathbf{r}_2), \ldots, f(\mathbf{r}_N)$. The problem is to compute the value of f at some arbitrary position $f(\mathbf{r})$ using the discrete values at particle locations inside of the $\mathbf{r}$ neighbourhood. To define the set of particles and the $\mathbf{r}$ neighbourhood, a weight function $\mathrm{w}(\mathbf{r} - \mathbf{r}_i)$ is introduced. Different weight functions have been used in the literature and the most common are the Gaussian and cubic spline functions, being the first one chosen in this paper as

$$\mathrm{w}_i = \mathrm{w}(\mathbf{r} - \mathbf{r}_i) = \begin{cases} e^{-\gamma \|\mathbf{r}-\mathbf{r}_i\|^2/h^2}, & \text{if } \frac{\|\mathbf{r}-\mathbf{r}_i\|}{h} \leq 1 \\ 0 & \text{else} \end{cases} \tag{16}$$

where $\mathbf{r}_i$ is the ith particle position inside the neighbourhood and h defines the interaction length between particles.

Considering a Taylor's series expansion of $f(\mathbf{r}_i)$ around $\mathbf{r}$

$$f(\mathbf{r}_i) = f(\mathbf{r}) + \sum_{k=1}^{3} f_k (r_{ki} - r_k) + \frac{1}{2} \sum_{k,l=1}^{3} f_{kl} (r_{ki} - r_k)(r_{li} - r_l) + \epsilon_i, \tag{17}$$

where ϵ_i is the truncation error of the Taylor's series expansion, r_{ki} and r_k represent the kth components of the position vectors $\mathbf{r}_i$ and $\mathbf{r}$, respectively. f_k and f_{kl} ($f_{kl} = f_{lk}$) represent the first and second spatial derivatives at particle position $\mathbf{r}$. The values of f_k and f_{kl} can be computed minimizing ϵ_i for the n_p Taylor's series expansion of $f(\mathbf{r}_i)$ corresponding to the n_p particles inside the $\mathbf{r}$ neighbourhood. This system of equations can be expressed in matrix form as

$$\epsilon = M\mathbf{a} - \mathbf{b}, \tag{18}$$

where

$$\epsilon = \left[\epsilon_1, \epsilon_2, \ldots, \epsilon_{n_p}\right]^t, \tag{19}$$

$$\mathbf{a} = [f, f_1, f_2, f_3, f_{11}, f_{12}, f_{13}, f_{22}, f_{23}, f_{33}]^t, \tag{20}$$

$$\mathbf{b} = \left[f(\mathbf{r}_1), f(\mathbf{r}_2), \ldots, f\left(\mathbf{r}_{n_p}\right)\right]^t, \tag{21}$$

$$M = \left[\mathbf{s}_1, \mathbf{s}_2, \ldots, \mathbf{s}_{n_p}\right]^t, \tag{22}$$

$$\mathbf{s}_i = [1, \Delta r_{1i}, \Delta r_{2i}, \Delta r_{3i}, \Delta r_{11i}, \Delta r_{12i}, \Delta r_{13i}, \Delta r_{22i}, \Delta r_{23i}, \Delta r_{33i}]^t, \tag{23}$$

Δr_{ki}, Δr_{kli} and Δr_{kki} are defined as $\Delta r_{ki} = r_{ki} - r_k$, $\Delta r_{kli} = (r_{ki} - r_k)(r_{li} - r_l)$ and $\Delta r_{kki} = (r_{ki} - r_k)(r_{ki} - r_k)/2$, for $k, l = 1, 2, 3$, $k \neq l$. The unknown vector $\mathbf{a}$ is computed through WLSM by minimizing the quadratic form

$$J = \sum_{i=1}^{n_p} \mathrm{w}_i \epsilon_i^2, \tag{24}$$

which reads

$$\left(M^t W M\right)\mathbf{a} = \left(M^t W\right)\mathbf{b}, \tag{25}$$

where $W = \mathrm{diag}(\mathrm{w}_1, \mathrm{w}_2, \ldots, \mathrm{w}_{n_p})$. From this equation

$$\mathbf{a} = \left(M^t W M\right)^{-1}\left(M^t W\right)\mathbf{b}. \tag{26}$$

In this way, the values of the function and its derivatives at particles $\mathbf{r}$ can be obtained. This approach let to compute the derivatives needed for the pressure and velocity fields corrections in (14) and (15).

3.1 FPM approach for general elliptic partial differential equations

Poisson equations such as (11) have been previously studied in Tiwari and Kuhnert [39]. This scheme eventually leads to the enhancement in this approximation and to a new formulation to solve general elliptic partial differential equations [42] as

$$Af + \mathbf{B} \cdot \nabla f + C\nabla^2 f = D \tag{27}$$

with Dirichlet or Neumann boundary conditions, $f = E$ or $\frac{\partial f}{\partial \mathbf{n}} = E$ on $\partial\Omega$, respectively. Following their works we present, for completeness, the corresponding FPM discretization under this setting.

In the FPM representation for a general elliptic equation, (27) must be taken together with the system of n_p Taylor's series expansion of $f(\mathbf{r}_i)$ around $\mathbf{r}$. In this case, the matrices we need to compute by each particle in Ω take the following form:
If $\mathbf{r}_i \in \Omega$, then

$$M = \left[\mathbf{s}_1, \mathbf{s}_2, \ldots, \mathbf{s}_{n_p}, \mathbf{s}_e\right]^t, \tag{28}$$

$$\mathbf{b} = \left[f(\mathbf{r}_1), f(\mathbf{r}_2), \ldots, f\left(\mathbf{r}_{n_p}\right), D\right]^t, \tag{29}$$

and

$$W = \operatorname{diag}\left(\mathrm{w}_1, \mathrm{w}_2, \ldots, \mathrm{w}_{n_p}, 1\right), \tag{30}$$

where

$$\mathbf{s}_e = [A, B_1, B_2, B_3, C, 0, 0, C, 0, C]^t. \tag{31}$$

If $\mathbf{r}_i \in \partial\Omega$, additionally we have to add the corresponding boundary conditions. In the case of Dirichlet boundary conditions, it is performed by adding the following rows to the matrices M and W, respectively,

$$(1, 0, 0, \ldots, 0), \quad (0, 0, 0, \ldots, 1) \tag{32}$$

whilst E is added to vector $\mathbf{b}$.

Similarly, in the case of Neumann boundary conditions we add the following rows to M and W, respectively,

$$(0, n_1, n_2, n_3, 0, \ldots, 0), \quad (0, 0, \ldots, 1) \tag{33}$$

where $\mathbf{n} = [n_1, n_2, n_3]^t$ denotes the outward orthonormal vector to the boundary, whilst E is added to vector $\mathbf{b}$.

Considering the moving least squares solution

$$\mathbf{a} = \left(M^t W M\right)^{-1} \left(M^t W\right) \mathbf{b}, \tag{34}$$

taking $\mathbf{q} = [q_1, q_2, \ldots, q_{10}]^t$ which denotes the first row of $\left(M^t W M\right)^{-1}$ and working out the terms in (34), we can see that the following linear equations arises

$$\begin{aligned} f\left(\mathbf{r}_j\right) - \sum_{i=1}^{n(j)} \mathrm{w}_i \, & (q_1 + q_2\Delta r_{1i} + q_3\Delta r_{2i} \\ & + q_4\Delta r_{3i} + q_5\Delta r_{11i} + q_6\Delta r_{12i} \\ & + q_7\Delta r_{13i} + q_8\Delta r_{22i} + q_9\Delta r_{23i} + q_{10}\Delta r_{33i}) \\ f(\mathbf{r}_i) = & [Aq_1 + B_1 q_2 \\ & + B_2 q_3 + B_3 q_4 + (q_5 + q_8 + q_{10})\, C]\, D \\ & + (n_1 q_2 + n_2 q_3 + n_3 q_4)\, E, \end{aligned} \tag{35}$$

where $f\left(\mathbf{r}_j\right)$ denotes the unknown function value at particle j and $n(j)$ the number of jth-particle neighbours. If the particle at $\mathbf{r}_j$ is on a Dirichlet boundary, (35) becomes $f\left(\mathbf{r}_j\right) = E$. Since Eq. 35 is valid for $j = 1, 2, \ldots, N$, this can be arranged in a full sparse system of linear equations $L\tilde{\mathbf{f}} = \mathbf{o}$ which can be solved by iterative methods. Thus, all kinds of Poisson equations such as (11) can be solved in this way, just adding appropriate entries in the systems of equations.

3.2 FPM formulation for coupled vector boundary value problems

The projection scheme detailed in the previous section involves the computation of an initial and vector boundary value problem for the intermediate velocity (10), whose general form is given by

$$A\mathbf{v}^* - B\nabla^2\mathbf{v}^* = \mathbf{C}, \tag{36}$$

and its boundary and initial conditions are given by (3)–(8). However, it must be noted that the boundary conditions on the free surface particles, (7) and (8), explicitly couple the components of $\mathbf{v}^*$. Therefore, its components cannot be computed separately through the previous FPM formulation for general elliptic partial differential equations because they require to be simultaneously computed.

Consequently, the FPM formulation proposed in Saucedo-Zendejo and Reséndiz-Flores [34] will be considered here to solve this coupled vector problem and with the aim to use the semi-implicit Chorin–Uzawa's projection scheme depicted in Sect. 2. Following [34], let $\mathbf{v}^*(\mathbf{r}_i) = \mathbf{v}_i = [v_{1i}, v_{2i}, v_{3i}]^t$ and $\mathbf{v}^*(\mathbf{r}) = \mathbf{v} = [v_1, v_2, v_3]^t$. The Taylor's series expansion

of each component of $\mathbf{v}_i$ around some arbitrary position $\mathbf{r}$ is:

$$v_{1i} = v_1 + \sum_{k=1}^{3} \frac{\partial v_1}{\partial r_k}(r_{ki} - r_k) + \frac{1}{2}\sum_{k,l=1}^{3} \frac{\partial^2 v_1}{\partial r_k \partial r_l}(r_{ki} - r_k)(r_{li} - r_l) + \epsilon_{1i}, \tag{37}$$

$$v_{2i} = v_2 + \sum_{k=1}^{3} \frac{\partial v_2}{\partial r_k}(r_{ki} - r_k) + \frac{1}{2}\sum_{k,l=1}^{3} \frac{\partial^2 v_2}{\partial r_k \partial r_l}(r_{ki} - r_k)(r_{li} - r_l) + \epsilon_{2i}, \tag{38}$$

$$v_{3i} = v_3 + \sum_{k=1}^{3} \frac{\partial v_3}{\partial r_k}(r_{ki} - r_k) + \frac{1}{2}\sum_{k,l=1}^{3} \frac{\partial^2 v_3}{\partial r_k \partial r_l}(r_{ki} - r_k)(r_{li} - r_l) + \epsilon_{3i}, \tag{39}$$

which form a system of $3n$ equations when (37)–(39) are taken for the n_p particles inside the neighbourhood of $\mathbf{r}$. Similar to Sect. 3.1, together with this system of $3n$ equations, the vector equation (36) must be satisfied in $\mathbf{r}$. Thus, the following three equations are added to the system of equations in order to impose this condition on $\mathbf{v}$,

$$Av_1 + B\left(\frac{\partial^2}{\partial r_1^2} + \frac{\partial^2}{\partial r_2^2} + \frac{\partial^2}{\partial r_3^2}\right) v_1 = C_1, \tag{40}$$

$$Av_2 + B\left(\frac{\partial^2}{\partial r_1^2} + \frac{\partial^2}{\partial r_2^2} + \frac{\partial^2}{\partial r_3^2}\right) v_2 = C_2, \tag{41}$$

$$Av_3 + B\left(\frac{\partial^2}{\partial r_1^2} + \frac{\partial^2}{\partial r_2^2} + \frac{\partial^2}{\partial r_3^2}\right) v_3 = C_3. \tag{42}$$

Furthermore, if $\mathbf{r}$ is on a free surface, $\mathbf{v}$ must satisfy the boundary conditions (7) and (8). Thus, the following equations must be added to the last system

$$n_1^2\frac{\partial v_1}{\partial r_1} + n_1 n_2\left(\frac{\partial v_1}{\partial r_2} + \frac{\partial v_2}{\partial r_1}\right) + n_1 n_3\left(\frac{\partial v_1}{\partial r_3} + \frac{\partial v_3}{\partial r_1}\right) + n_2^2\frac{\partial v_2}{\partial r_2} + n_2 n_3\left(\frac{\partial v_2}{\partial r_3} + \frac{\partial v_3}{\partial r_2}\right) + n_3^2\frac{\partial v_3}{\partial r_3} = \frac{1}{2\nu\rho}H, \tag{43}$$

$$2n_1 t_{i_1}\frac{\partial v_1}{\partial r_1} + \left(n_1 t_{i_2} + n_2 t_{i_1}\right)\left(\frac{\partial v_1}{\partial r_2} + \frac{\partial v_2}{\partial r_1}\right) + \left(n_1 t_{i_3} + n_3 t_{i_1}\right)\left(\frac{\partial v_1}{\partial r_3} + \frac{\partial v_3}{\partial r_1}\right) + 2n_2 t_{i_2}\frac{\partial v_2}{\partial r_2} + \left(n_2 t_{i_3} + n_3 t_{i_2}\right)\left(\frac{\partial v_2}{\partial r_3} + \frac{\partial v_3}{\partial r_2}\right) + 2n_3 t_{i_3}\frac{\partial v_3}{\partial r_3} = 0, \tag{44}$$

where $H = p^n - \sigma\kappa$ and $t_i = [t_{i_1}, t_{i_2}, t_{i_3}]^t$ for $i = 1, 2$. In the case that $\mathbf{r}$ is on a different boundary condition, it must satisfy the corresponding condition from (3)–(6). Thus, it has a system of $3n_p + 3$ linear equations for inner particles and a system of $3n_p + 6$ linear equations for boundary particles in order to compute 30 unknowns, the components of $\mathbf{v}$ and their first and second spacial derivatives.

Considering that $\mathbf{r}$ is on a free surface, the system of $3n_p + 6$ equations can be expressed in matrix form as

$$\epsilon = M^*\mathbf{a} - \mathbf{b}, \tag{45}$$

where

$$\epsilon = \left[\epsilon_{11}, \epsilon_{12}, \ldots, \epsilon_{1n_p}, \epsilon_{21}, \epsilon_{22}, \ldots, \epsilon_{2n_p}, \epsilon_{31}, \epsilon_{32}, \ldots, \epsilon_{3n_p}, 0, 0, 0, 0, 0, 0\right]^t, \tag{46}$$

$$\mathbf{b} = \left[v_{11}, v_{12}, \ldots, v_{1n_p}, v_{21}, v_{22}, \ldots, v_{2n_p}, v_{31}, v_{32}, \ldots, v_{3n_p}, C_1, C_2, C_3, \frac{1}{2\nu\rho}H, 0, 0\right]^t, \tag{47}$$

$$\mathbf{a} = [\mathbf{k}_1, \mathbf{k}_2, \mathbf{k}_3]^t, \tag{48}$$

$$M^* = \begin{pmatrix} M & Z & Z \\ Z & M & Z \\ Z & Z & M \\ Y_1 & Y_2 & Y_3 \end{pmatrix}, \tag{49}$$

where Z is a matrix of zeros, M is given by (22) and

$$\mathbf{k}_i = \left[v_i, \frac{\partial v_i}{\partial r_1}, \frac{\partial v_i}{\partial r_2}, \frac{\partial v_i}{\partial r_3}, \frac{\partial^2 v_i}{\partial r_1^2}, \frac{\partial^2 v_i}{\partial r_1 \partial r_2}, \frac{\partial^2 v_i}{\partial r_1 \partial r_3}, \frac{\partial^2 v_i}{\partial r_2^2}, \frac{\partial^2 v_i}{\partial r_2 \partial r_3}, \frac{\partial^2 v_i}{\partial r_3^2}\right]^t, \tag{50}$$

$$Y_1 = \begin{pmatrix} A & 0 & 0 & 0 & B\,0\,0\,B\,0\,B \\ 0 & 0 & 0 & 0 & 0\,0\,0\,0\,0\,0 \\ 0 & 0 & 0 & 0 & 0\,0\,0\,0\,0\,0 \\ 0 & n_1^2 & n_1 n_2 & n_1 n_3 & 0\,0\,0\,0\,0\,0 \\ 0 & 2n_1 t_{1_1} & n_1 t_{1_2} + n_2 t_{1_1} & n_1 t_{1_3} + n_3 t_{1_1} & 0\,0\,0\,0\,0\,0 \\ 0 & 2n_1 t_{2_1} & n_1 t_{2_2} + n_2 t_{2_1} & n_1 t_{2_3} + n_3 t_{2_1} & 0\,0\,0\,0\,0\,0 \end{pmatrix}, \tag{51}$$

$$Y_2 = \begin{pmatrix} 0 & 0 & 0 & 0 & 0\,0\,0\,0\,0\,0 \\ A & 0 & 0 & 0 & B\,0\,0\,B\,0\,B \\ 0 & 0 & 0 & 0 & 0\,0\,0\,0\,0\,0 \\ 0 & n_1 n_2 & n_2^2 & n_2 n_3 & 0\,0\,0\,0\,0\,0 \\ 0 & n_1 t_{1_2} + n_2 t_{1_1} & 2n_2 t_{1_2} & n_2 t_{1_3} + n_3 t_{1_2} & 0\,0\,0\,0\,0\,0 \\ 0 & n_1 t_{2_2} + n_2 t_{2_1} & 2n_2 t_{2_2} & n_2 t_{2_3} + n_3 t_{2_2} & 0\,0\,0\,0\,0\,0 \end{pmatrix}, \tag{52}$$

$$Y_3 = \begin{pmatrix} 0 & 0 & 0 & 0 & 0\,0\,0\,0\,0\,0 \\ 0 & 0 & 0 & 0 & 0\,0\,0\,0\,0\,0 \\ A & 0 & 0 & 0 & B\,0\,0\,B\,0\,B \\ 0 & n_1 n_3 & n_2 n_3 & n_3^2 & 0\,0\,0\,0\,0\,0 \\ 0 & n_1 t_{1_3} + n_3 t_{1_1} & n_2 t_{1_3} + n_3 t_{1_2} & 2n_3 t_{1_3} & 0\,0\,0\,0\,0\,0 \\ 0 & n_1 t_{2_3} + n_3 t_{2_1} & n_2 t_{2_3} + n_3 t_{2_2} & 2n_3 t_{2_3} & 0\,0\,0\,0\,0\,0 \end{pmatrix}. \tag{53}$$

Therefore, similar to the procedure followed previously, the moving least squares solution reads

$$\mathbf{a} = \left(M^{*t} W M^*\right)^{-1}\left(M^{*t} W\right)\mathbf{b}, \tag{54}$$

where $W = \text{diag}\left(\text{w}_1, \text{w}_2, \ldots, \text{w}_{n_p}, \text{w}_1, \text{w}_2, \ldots, \text{w}_{n_p}, \text{w}_1, \text{w}_2, \ldots, \text{w}_{n_p}, 1, 1, 1, 1, 1, 1\right)$. For the special case of inner particles, the last three rows in M^* and W, as well as the last three components of $\mathbf{b}$ are omitted.

It must be noticed that only the first, eleventh and twenty-first components of $\mathbf{a}$ are required for the computation of $\mathbf{v}^*$ in (36) instead of the full vector. Thus, similar to the procedure depicted in Sect. 3.1, by taking $\mathbf{q}_i = [q_{i,1}, q_{i,2}, \ldots, q_{i,30}]^t$ which denotes the ith row of $\left(M^{*t} W M^*\right)^{-1}$ and working out the terms in (54), we can see that the following linear equations arise from the first, eleventh and twenty-first components of $\mathbf{a}$

$$
\begin{aligned}
& v_{mj} - \sum_{i=1}^{n(j)} w \left[\left(q_{p,1} + q_{p,2}\Delta r_{1i} + q_{p,3}\Delta r_{2i} + q_{p,4}\Delta r_{3i} \right.\right. \\
& \quad + q_{p,5}\Delta r_{11i} + q_{p,6}\Delta r_{12i} \\
& \quad \left.\left. + q_{p,7}\Delta r_{13i} + q_{p,8}\Delta r_{22i} + q_{p,9}\Delta r_{23i} + q_{p,10}\Delta r_{33i} \right) v_{1i} \right. \\
& \quad + \left(q_{p,11} + q_{p,12}\Delta r_{1i} \right. \\
& \quad + q_{p,13}\Delta r_{2i} + q_{p,14}\Delta r_{3i} + q_{p,15}\Delta r_{11i} \\
& \quad + q_{p,16}\Delta r_{12i} + + q_{p,17}\Delta r_{13i} + q_{p,18}\Delta r_{22i} \\
& \quad \left. + q_{p,19}\Delta r_{23i} + q_{p,20}\Delta r_{33i} \right) v_{2i} \\
& \quad + \left(q_{p,21} + q_{p,22}\Delta r_{1i} + q_{p,23}\Delta r_{2i} + q_{p,24}\Delta r_{3i} \right. \\
& \quad + q_{p,25}\Delta r_{11i} + q_{p,26}\Delta r_{12i} + q_{p,27}\Delta r_{13i} \\
& \quad \left. \left. + q_{p,28}\Delta r_{22i} + q_{p,29}\Delta r_{23i} + q_{p,30}\Delta r_{33i} \right) v_{3i} \right] \\
& = \left[A q_{p,1} + \left(q_{p,5} + q_{p,8} + q_{p,10} \right) B \right] C_1 \\
& \quad + \left[A q_{p,11} + \left(q_{p,15} + q_{p,18} + q_{p,20} \right) B \right] C_2 \\
& \quad + \left[A q_{p,21} + \left(q_{p,25} + q_{p,28} + q_{p,30} \right) B \right] C_3 \\
& \quad + \frac{1}{2\nu\rho} \left[n_1^2 q_{p,2} + n_1 n_2 \left(q_{p,3} + q_{p,12} \right) \right. \\
& \quad + n_1 n_3 \left(q_{p,4} + q_{p,22} \right) \\
& \quad \left. + n_2^2 q_{p,13} + n_2 n_3 \left(q_{p,14} + q_{p,23} \right) + n_3^2 q_{p,24} \right] H, \qquad (55)
\end{aligned}
$$

where $j = 1, 2, \ldots, N$, $m = 1, 2, 3$ and $p = 1, 11, 21$. This system of linear equations can be arranged in a full sparse system $L\tilde{\mathbf{v}} = \mathbf{o}$ which can be solved by iterative methods.

Therefore, any coupled vector boundary value problem as (10) could be solved with this formulation, and hence the semi-implicit Chorin–Uzawa's projection scheme depicted in Sect. 2 is solved suitably and easily with FPM.

4 Implementation aspects

With all the previous theories to numerically solve the free surface flows during mould filling with FPM already depicted, it is necessary to point out some important implementation aspects. They refer to the free surface and inflow particles treatment and to the isolated particles handling.

4.1 Detection of free surface particles

In this work, the free surface particles are detected following the approach proposed in Tiwari and Kuhnert [40]. A particle is on a free surface if it lies on the interface between a void space region and a region with inner and other kinds of boundary particles. Thus, a particle in an arbitrary position $\mathbf{r}$ is a free surface particle if it is possible to find a sphere which fulfils:

1. The radius of this sphere is $r_{fs} = \varphi h$, where $\varphi \in [0.6, 1.0]$ and h is the smoothing length.
2. This sphere is void.

These conditions let to guarantee that if such void sphere exists, the particle at $\mathbf{r}$ lies on a free surface. Consequently, an inner particle cannot locate a sphere with a larger or equal radius to r_{fs} because it would indicate that there is a big hole in the discretized domain. To locate a void sphere, it is required to execute a discrete search over all the possible directions around each particle position $\mathbf{r}$. This involves a great computational cost for the free surface particles detection. Nevertheless, a discrete search over all the inner particles is required only at the simulation start or in the first time step because in the following time steps the discrete search could be performed only around neighbouring inner particles close to particles that were on a surface boundary in the last time step. Such strategy allows decreasing the required computational cost for the detection of these kinds of particles.

4.2 Inflow boundary treatment

The inflow boundary condition exists on a virtual surface of the domain through which the fluid enters. This surface is identified before starting the simulation process such that at the beginning of the simulation process, a set of inflow particles are generated on this surface, which are moved according to the numerical algorithm shown in Sect. 2, and thus they must fulfil the conditions (3) and (12).

Since these are moving through time, they quickly become inner particles when they surpass a certain and small distance from the inflow virtual surface. Therefore, in this case a new set of inflow particles are generated on such virtual surface and this procedure is repeated throughout the simulation until the mould is completely filled. This totally filled condition occurs when it is no longer possible to detect free surface particles, which indicates that the mould is completely filled.

4.3 Computation of normal vector on free surface

Once the particle on free surfaces has been detected through the previous approach, it is needed to compute the outward

normal vectors to the free surface at these particles since they are required in the boundary conditions. They are computed following the algorithm proposed in algorithm proposed in Reséndiz-Flores et al [32]. Thus, we are interested in computing the outward normal vector $\mathbf{n}$ to the free surface at the particle $\mathbf{r}_i$. Therefore, let $\mathbf{r}_j$ be one of the N_b free surface particles in a neighbourhood defined by a weight function ω_{ij}. The weight function ω_{ij} can be quite arbitrary; however, in this work we consider again a Gaussian weight function. Consequently, the angle $\cos\alpha_{ij}$ between the normal and the vector $\mathbf{r}_j - \mathbf{r}_i$ satisfies

$$\cos\alpha_{ij} = \frac{\mathbf{n}\cdot\left(\mathbf{r}_j - \mathbf{r}_i\right)}{\left\|\mathbf{r}_j - \mathbf{r}_i\right\|\|\mathbf{n}\|}. \tag{56}$$

Moreover, the following quadratic form arises

$$\cos^2\alpha_{ij} = \frac{\mathbf{n}^{\mathrm{T}}\left(\mathbf{r}_j - \mathbf{r}_i\right)\left(\mathbf{r}_j - \mathbf{r}_i\right)^{\mathrm{T}}\mathbf{n}}{\left\|\mathbf{r}_j - \mathbf{r}_i\right\|^2}. \tag{57}$$

If all the boundary particles in the neighbourhood of $\mathbf{r}_i$ are considered, we have

$$\sum_j \cos^2\alpha_{ij}\omega_{ij} = \mathbf{n}^{\mathrm{T}}\sum_j\left(\frac{\left(\mathbf{r}_j - \mathbf{r}_i\right)\left(\mathbf{r}_j - \mathbf{r}_i\right)^{\mathrm{T}}\omega_{ij}}{\left\|\mathbf{r}_j - \mathbf{r}_i\right\|^2}\right)\mathbf{n}. \tag{58}$$

Defining

$$C = \sum_j\left(\frac{\left(\mathbf{r}_j - \mathbf{r}_i\right)\left(\mathbf{r}_j - \mathbf{r}_i\right)^{\mathrm{T}}\omega_{ij}}{\left\|\mathbf{r}_j - \mathbf{r}_i\right\|^2}\right), \tag{59}$$

Equation (58) can be expressed as

$$\sum_j \cos^2\alpha_{ij}\omega_{ij} = \mathbf{n}^{\mathrm{T}}C\mathbf{n}, \tag{60}$$

hence, the outward normal vector $\mathbf{n}$ is automatically obtained when the following optimal problem is solved

$$\min_{\mathbf{n}\in\mathbb{R}^3,\|\mathbf{n}\|=1}\sum_j \cos^2\alpha_{ij}\omega_{ij} = \min_{\mathbf{n}\in\mathbb{R}^3,\|\mathbf{n}\|=1}\mathbf{n}^{\mathrm{T}}C\mathbf{n}, \tag{61}$$

which leads to the following eigenvalue problem

$$C\mathbf{n} = \beta\mathbf{n}. \tag{62}$$

4.4 Handling of isolated particles

A simple problem arises when the amount of particles within the neighbourhood of a particle is less than the unknowns to be solved in FPM. This is more frequent in boundary particles because they are not completely surrounded by other particles. Thus, an isolated particle is defined as that particle which has less neighbour particles than the unknowns to be computed. Commonly, the isolated particles are those regions of a fluid which were splashed or sprayed.

There are two approaches to solve the problem with isolated particles that depend on the importance of these particles:

1. If the isolated particles are not so important for the global solution, they could be deleted.
2. If the isolated particles are important in the global solution, it is required to reduce the approximation order in the Taylor's series expansions (17), (37), (38) and (39) which decreases the unknowns number and the number of neighbours required for the solution. If this method is performed and a particle is still isolated, its velocity could be computed through the kinematic equation

$$\mathbf{v}^{n+1} = \mathbf{v}^n + \Delta t\mathbf{f}^{n+1} \tag{63}$$

and its pressure could be taken as the atmospheric one.

For sake of simplicity, in the numerical examples in this work the first strategy to deal with isolated particles will be taken.

5 Numerical results

In this section, the suitability and feasibility of this semi-implicit FPM formulation to predict three-dimensional free surface flows in mould filling processes will be shown. For this, the simulations of some 3D test examples using this meshfree approach are reported.

5.1 Circular mould with core

In order to evaluate the capability of this semi-implicit FPM formulation to simulate 3D complex mould filling processes, the filling of the classical circular mould with core benchmark will be considered as a first example since numerical and experimental results are available [13,30,35,41,43]. Schmid and Klein experimentally studied the filling pattern of this mould using water at room temperature [35]. Therefore, the numerical filling patterns predicted with the proposed FPM formulation will be compared here with the experimental results in Schmid and Klein [35] and with the numerical results obtained in Ren et al. [30] and in Xu and Yu [43] with improved SPH methods. The geometry of the circular mould with core is shown in Fig. 1.

Three different simulations were carried out considering three discretizations with 57,000, 230,000 and 1,000,000 par-

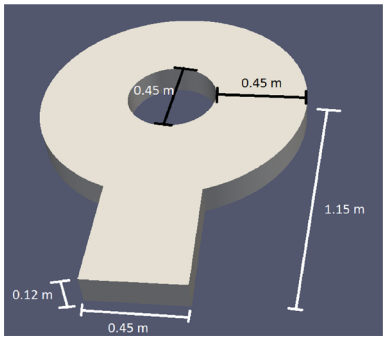

Fig. 1 Circular mould with core

ticles, approximately, with a mean spacing of 0.016, 0.008 and 0.004 m with the aim of studying convergence. The smoothing length used with each of these discretizations was 0.053, 0.0264 and 0.0132 m, respectively. In all these cases, the inflow velocity was considered as $\mathbf{v} = [0, 0, 18\ \mathrm{m/s}]^t$. The pressure in all particles and the atmospheric pressure were taken as zero. The surface tension forces and the gravitational acceleration vector were neglected. The viscosity and the density of the fluid were considered as $\nu = 0.01\,\mathrm{m}^2/\mathrm{s}$ and $\rho = 1000\,\mathrm{kg/m}^3$, respectively. Finally, a slip boundary condition was imposed at solid walls and the time step was taken as $\Delta t = 0.0002\,\mathrm{s}$.

These simulations were performed on a i7-6700 CPU 3.4 GHz processor running Linux Mint 18.2 operating system with 32 GB of RAM. The computing time elapsed for each discretization was 18 h, 53 h and 225 h.

The simulation results of these simulations are depicted in Fig. 2. These pictures show that there is no significant gain in accuracy by increasing the number of particles for the simulation and that the coarsest discretization considered here is sufficient to study the filling pattern of this mould since there are no significant differences between the three discretization for the filling pattern; and further, the three simulations show a smooth and stable evolution of the domain through time.

A comparison of the filling patterns predicted by this FPM formulation with the discretization of 57,000 particles with the numerical and experimental results studied in [35], and the numerical results in Ren et al. [30] and in Xu and Yu [43] at different time steps are shown in Fig. 3. As it can be seen in this picture, the numerical results predicted by this FPM approach match very well with their experimental counterparts, in the free surface patterns and the domain evolution over time. Comparisons among the numerical results show that this FPM formulation and the SPH methods are stable for the simulation of complex mould filling processes. However, here it can also be noted that, in contrast to the FPM simulation, the Ren's SPH simulation shows slight instabilities which spread on the free surfaces and the Xu's SPH simulation shows a filling profile slightly different from the experimental one in the fluid fronts that travel through the lower part of the outer disc; and further, both SPH simulations show a perfectly symmetric filling pattern that is not observed in the experimental profile. Thus, FPM is more stable and reliable than these SPH approaches for the simulation of complex mould filling processes. Therefore, these results indicate the attractiveness and accuracy of this FPM formulation for the numerical simulation of 3D complex mould filling processes in metal casting. For further validation examples with this FPM formulation for free surface fluid flows, we refer to the numerical examples in [31,34].

In order to further show the feasibility and suitability of this semi-implicit FPM formulation for the numerical prediction of 3D free surface flows in mould filling processes, the numerical simulation of three additional examples will be presented in the following subsections. These cases are similar to those arising in real casting processes. They correspond to the geometries sketched in Fig. 4.

5.2 Car rim

The chosen geometry for this test is shown in Fig. 4a), and it corresponds to a simplified model of an aluminium alloy car rim 19/215. In this example, the problem domain was discretized with approximately 230,000 particles with a mean spacing of 0.0047 m. The smoothing length for this simulation was taken as $h = 0.0141$ m. The inlet velocity was considered as $\mathbf{v} = [0, 0, 0.05\ \mathrm{m/s}]^t$. The pressure in all particles and the atmospheric pressure were taken as zero. The surface tension forces and the gravitational acceleration vector were neglected. The viscosity and density of the fluid were considered as $\mu = 0.01\,\mathrm{Pa\,s}$ and $\rho = 2982\,\mathrm{kg/m}^3$, respectively. These parameters corresponds to the physical parameters of the molten aluminium. Finally, similar to the previous example, a slip boundary condition was imposed at solid walls and the time step was taken as $\Delta t = 0.01\,\mathrm{s}$.

This simulation was performed on a i7-6700 CPU 3.4 GHz processor running Red Hat Enterprise Linux 7.3 operating system with 16 GB of RAM. The computing time elapsed for this simulation was 56 h.

Two perspective views of the filling patterns at different time steps are depicted in Fig. 5. There, the picture on the left shows the view from the top at some angle to one side, whilst the second one shows the view exactly from below. As it can be observed in this figure, the initial jet impacts the centre cap and then it is divided into five jets travelling on the spokes. These five jets impact then the barrel and next the liquid spread on this surface until it impacts the back flange. A rolling wave is formed here, and thus, the liquid starts to move and spread on the outer lip until all the rim wide area is completely filled. Finally, five rolling waves are formed on the spokes where the liquid travels until it reaches the

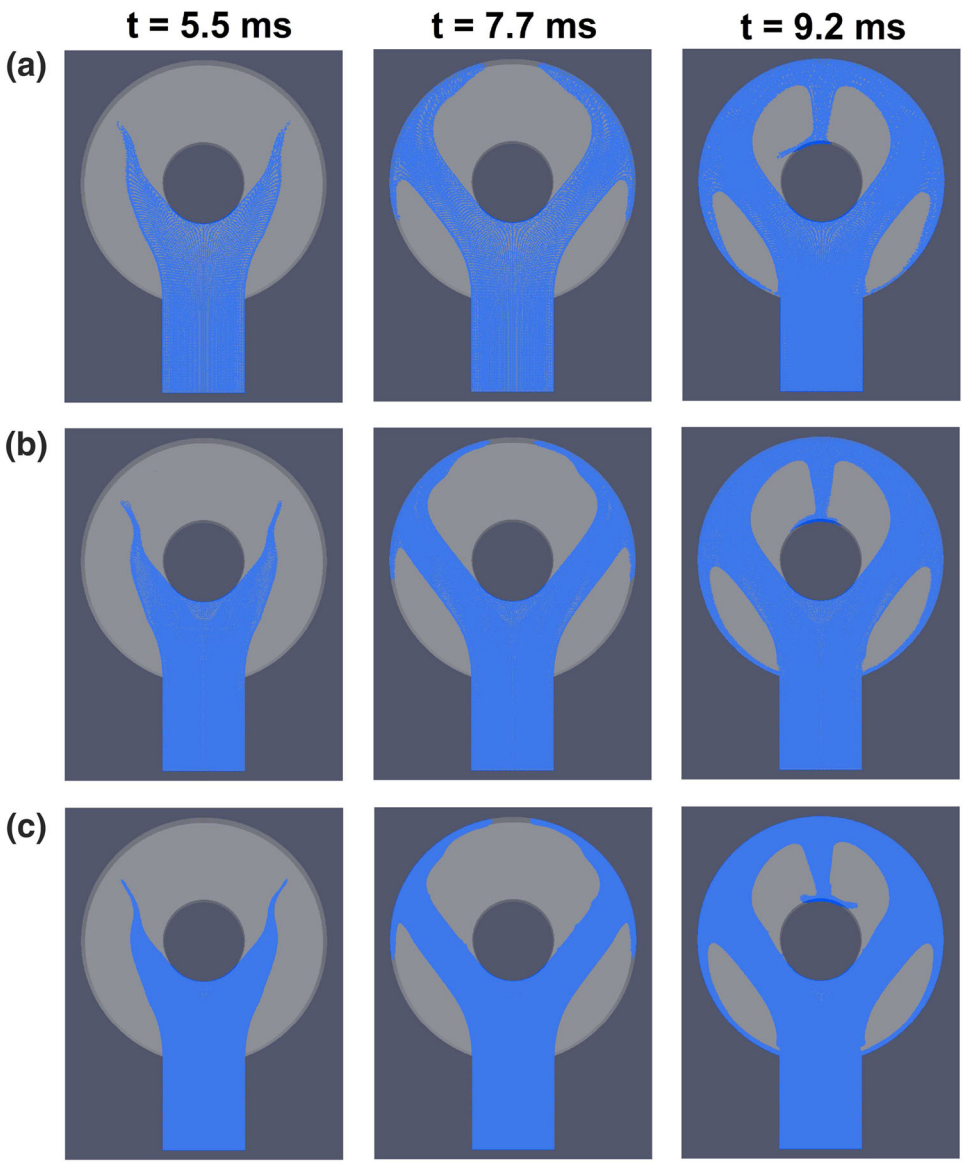

Fig. 2 Filling patterns at different time instances computed with FPM with **a** 57,000, **b** 230,000 and **c** 1,000,000 particles, respectively

initial jet, finishing the mould filling. The simulation results of this 3D mould filling process show the feasibility of this FPM formulation since the filling pattern evolution is quite smooth and it is clearly able to handle high deformations in the domain, the collision and the merger of liquid fronts, rolling and breaking waves.

5.3 Machine component

The third numerical test that was considered here corresponds to the machine component shown in Fig. 4b). It is one of the numerical test cases considered in Cleary and Ha [6], Cleary and Ha [7]. In this case, the problem domain was discretized with around 250,000 particles with a mean spacing of 0.00625 m. The smoothing length for this simulation was taken as $h = 0.02$ m. The hypothetical inlet velocity was considered as $\mathbf{v} = [0, 0, 0.08\,\text{m/s}]^t$. Anew, the pressure in all particles and the atmospheric pressure were taken as zero. The surface tension forces and the gravitational acceleration vector were neglected. The viscosity and density of the fluid were considered as $\mu = 0.01\,\text{Pa s}$ and $\rho = 2982\,\text{kg/m}^3$, respectively. Finally, similar to the previous examples, a slip boundary condition was imposed at solid walls and the time step was considered as $\Delta t = 0.01$ s.

This simulation was performed on a i7-6700 CPU 3.4 GHz processor running Red Hat Enterprise Linux 7.3 operating system with 16 GB of RAM. The computing time elapsed for this simulation was 59 h.

One more time, two perspective views of the filling patterns at different time steps are depicted in Fig. 6. There, the picture on the left shows the view from behind at some angle to one side and to the top, whilst the second one shows

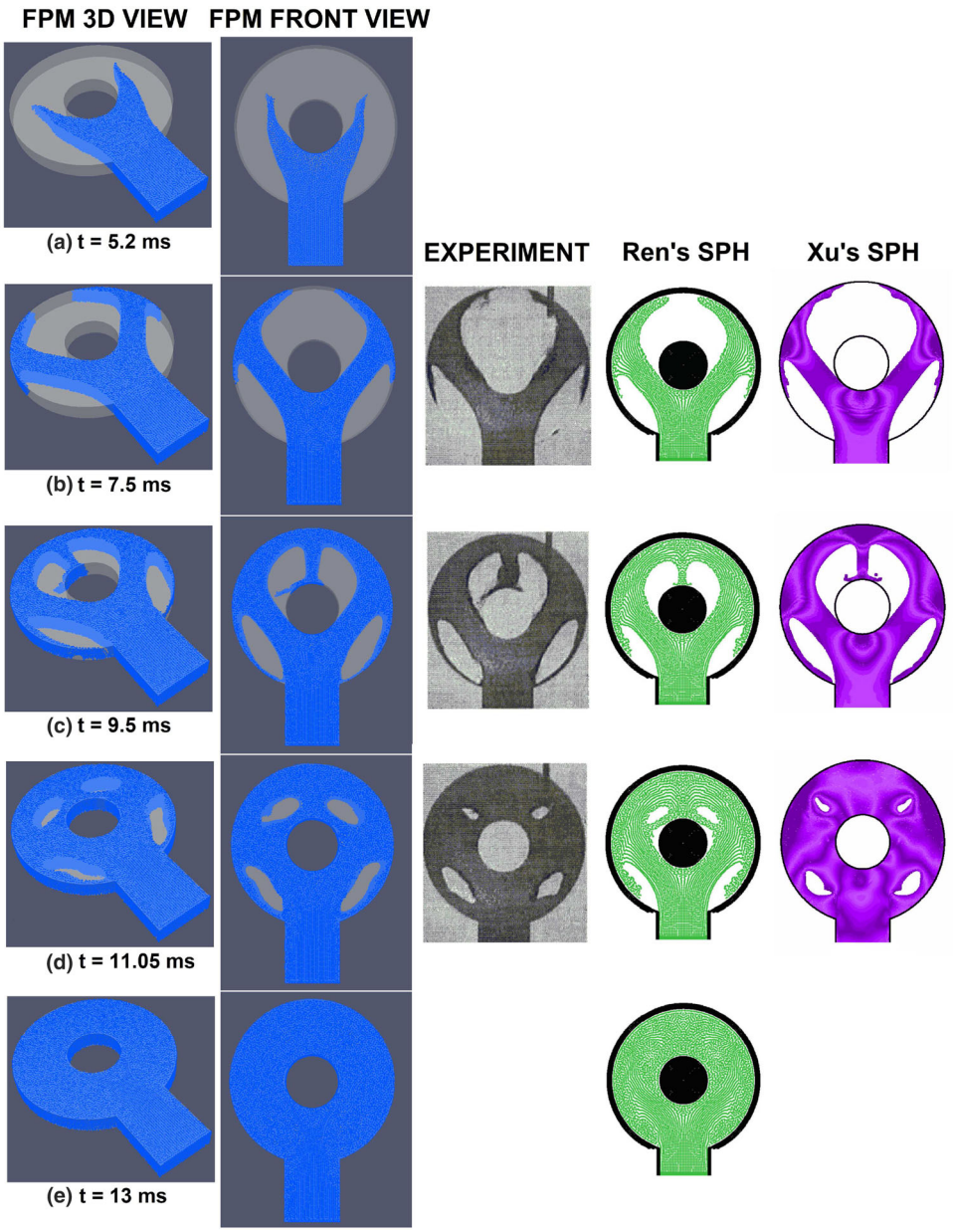

Fig. 3 Filling patterns through time. *First column* FPM 3D View. *Second column* FPM front view. *Third column* the experimental pattern in Ref. [35]. *Fourth column* SPH in Ref. [30]. *Fifth column* SPH in Ref. [43]

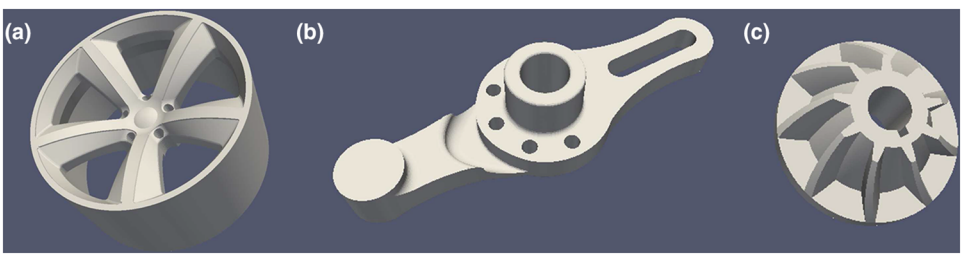

Fig. 4 Mould geometries

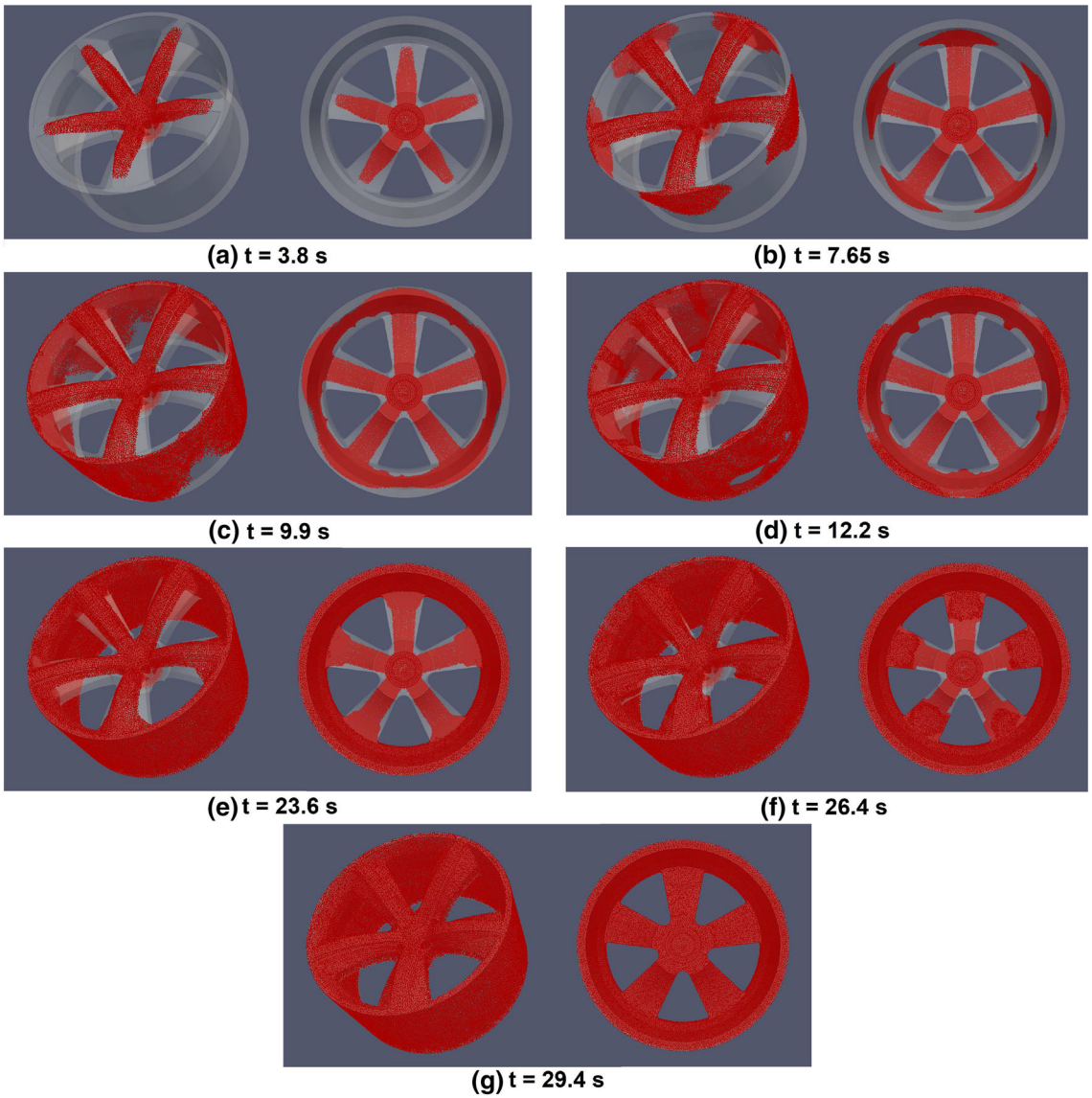

Fig. 5 Numerical filling patterns at different time steps

the view exactly from the top. As it is shown in this figure, the leading material is divided in four liquid fronts when it impacts three of the five cylindrical obstacles in the mould and starts to flow between them. Next, the two central liquid fronts impact the annular central section of the die where these jets partially merge forming a fifth liquid front which moves backwards. This jet finally fills the space between the original central fronts. In the annular central section of the mould, the liquid flows up into the upper extension. Regarding the two external liquid fronts, they flow around the curved outsides of the die until they collide with the fronts coming from the annular section. At this point, the fluid flow is mostly upwards around the upper extension of the annular section and around the curved outer parts of the die cavity towards the rear. Splashing droplets and liquid fragmentations are visible in the non-filled rear part of the mould, just behind the annular section. The fluid flow continues until the liquid fronts in the rear part of the die merge and the annular central section is substantially filled. Afterwards, almost all the mould cavities are filled and the biggest voids are principally behind two of the cylindrical obstacles and behind the annular section where the splashments occurred before. They are uniformly filled until the filling process finishes.

These pictures show the robustness of this FPM semi-implicit formulation for the simulation of complex 3D mould filling processes since the splashing into droplets, the fluid fragmentation into jets and the fronts collisions observed in this example are well reproduced and predicted by this

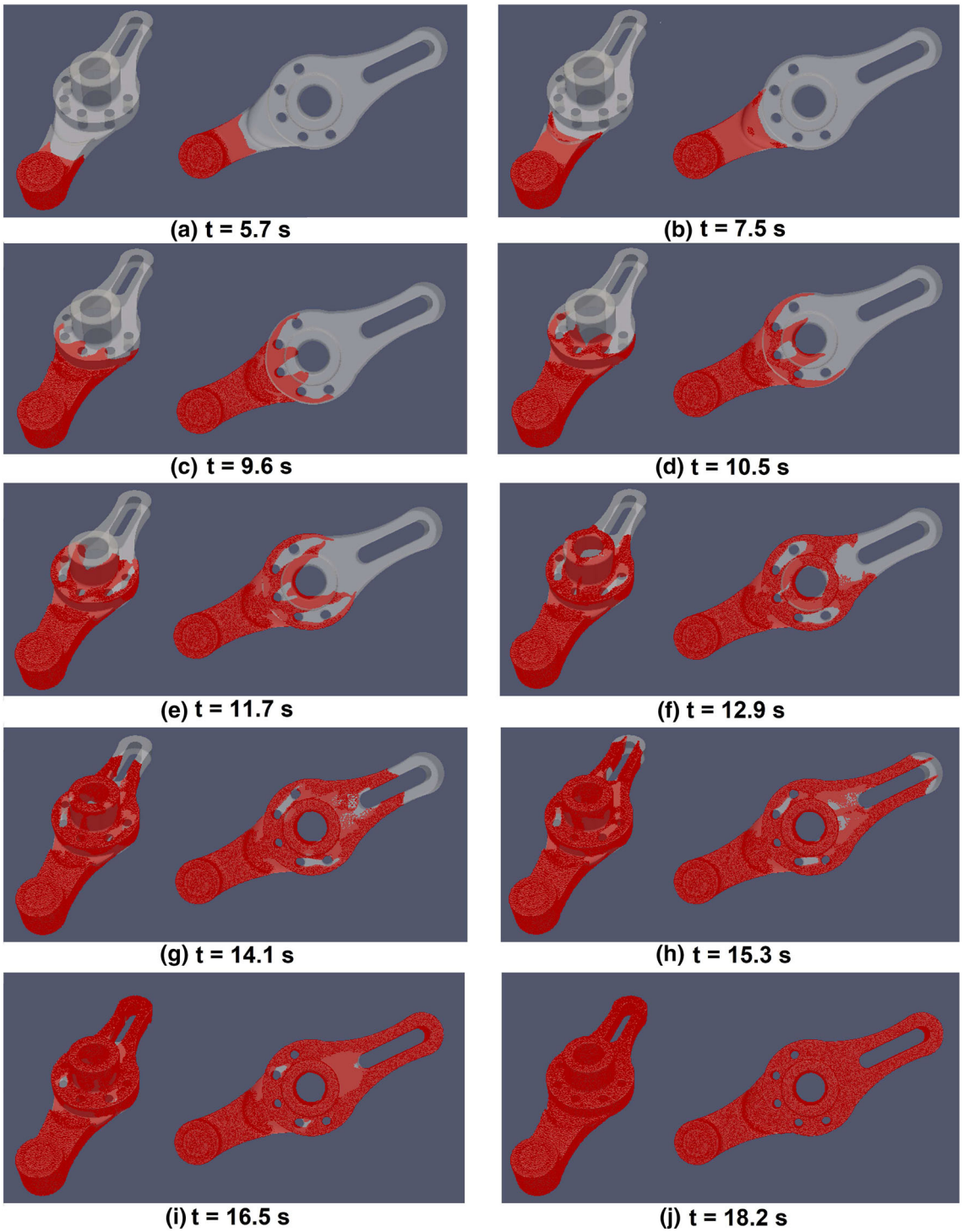

Fig. 6 Numerical filling patterns at different time steps

approach. This figure shows too the suitability of this formulation for dealing with these kinds of processes since it exhibits a smooth evolution over time and it does not show instabilities on the free surfaces or dispersed particles.

5.4 Turbine rotor

The final mould that was considered in this work corresponds to the turbine rotor shown in Fig. 4c). In this example, four inlet gates are considered which are equidistant from the rotor centre. There, the problem domain was discretized with approximately 260,000 particles with a mean spacing of 0.02 m. The smoothing length in this simulation was taken as $h = 0.062$ m. The hypothetical inlet velocity was considered as $\mathbf{v} = [0, 0, 0.04\ \text{m/s}]^t$. One more time, the pressure in all particles and the atmospheric pressure were taken as zero. The surface tension forces and the gravitational acceleration vector were neglected. The viscosity and density of the fluid were considered as $\mu = 0.001$ Pa s and $\rho = 1000\,\text{kg/m}^3$, respectively. Finally, similar to the previous examples, a slip boundary condition was imposed at solid walls and the time step was taken as $\Delta t = 0.05$ s.

This simulation was performed on a i7-6700 CPU 3.4 GHz processor running Linux Mint 18.2 operating system with 32 GB of RAM. The computing time elapsed for this simulation was 52 h.

Again, two perspective views of filling patterns at different time steps are depicted in Fig. 7. There, the picture on left shows the view from the top at some angle to one side, whilst the second one shows the view exactly from one side. As it can be seen in this figure, the action of the four inlets is an effective mould filling since the four initial jets substantially fill the upper part of the die; and once they strike the mould walls, the liquid fronts are spread towards the remaining void regions until a complete filling of the mould is achieved.

All these sets of figures show the suitability and feasibility of this FPM semi-implicit formulation since it performs well for the prediction of 3D free surface flows in mould filling processes. Further, they show that it is able to reproduce high deformations in the domain, the collision and the merger of

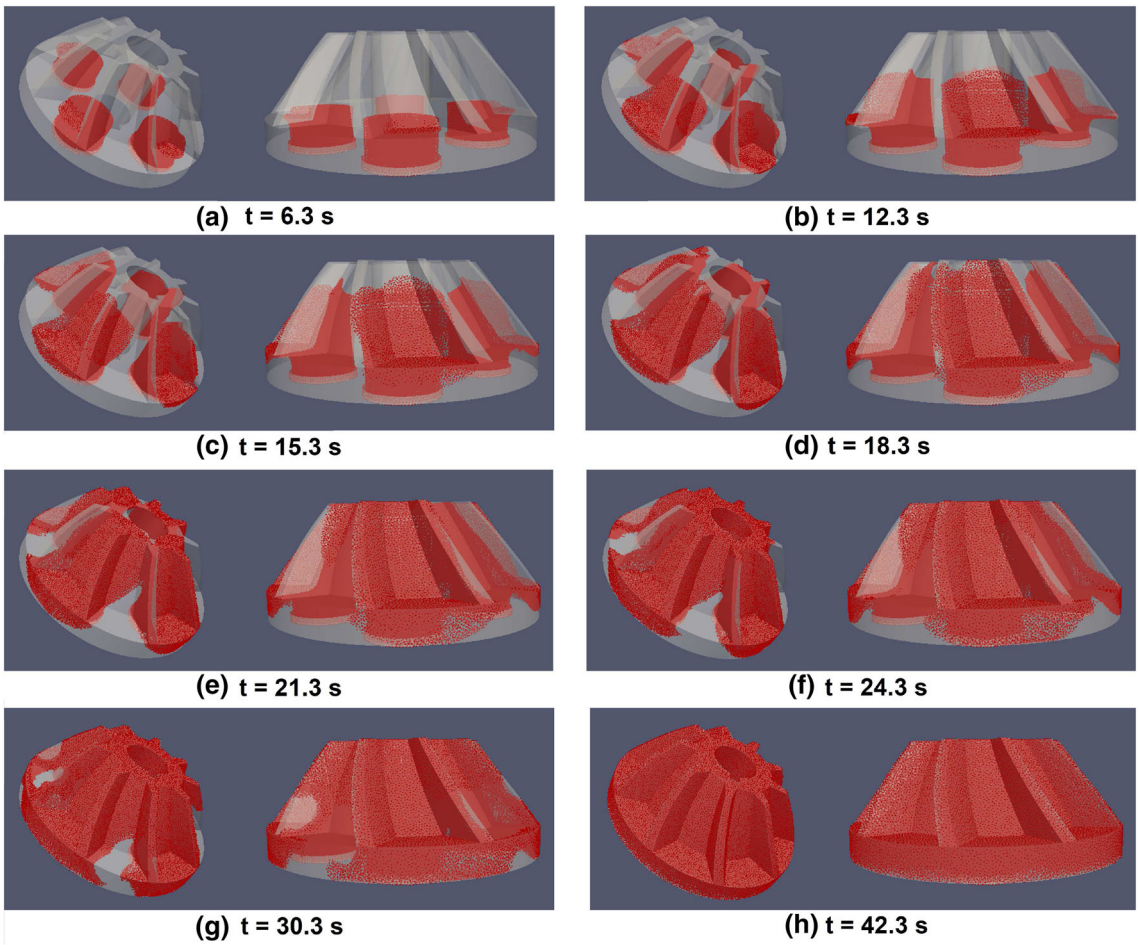

Fig. 7 Numerical filling patterns at different time steps

liquid fronts, rolling and breaking waves during the filling, and therefore, it constitutes a promising and powerful numerical tool in metal casting.

6 Conclusions

The discussed semi-implicit FPM formulation was successfully implemented and tested for the prediction of mould filling processes in casting. Taking into account the results from the numerical examples, we can conclude that the current FPM formulation has shown an excellent behaviour for the numerical simulation of these kinds of processes since the free surface flow patterns evolved in a reasonable manner according to the physical configurations over time. Therefore, it is suitable and feasible for the numerical simulation of 3D mould filling processes in metal casting where high deformations in the domain, the collision and the merger of liquid fronts, rolling and breaking waves take place.

Since this formulation is a truly meshfree method, it does not need to keep a regular point distribution to obtain good numerical solutions, not even to compute some numerical quadratures as in other numerical methods. This represents a considerable advantage regarding computational efficiency; and further, adaptive schemes can be easily developed. Moreover, it is simple to naturally incorporate any kind of boundary condition without requiring any special treatment or stabilization and it is really simple to implement. Therefore, it could be a promising and robust numerical tool for the prediction of 3D free surface flows in mould filling processes and in other industrial processes where complicated free surface flows take place.

Compliance with ethical standards

Conflict of interest On behalf of all authors, the corresponding author states that there is no conflict of interest.

References

1. Acevedo-Malavé A, García-Sucre M (2012) Many drops interactions I: simulation of coalescence, flocculation and fragmentation of multiple colliding drops with smoothed particle hydrodynamics. J Comput Multiph Flows 4(2):121–133
2. Bašić H, Demirdžić I, Muzaferija S (2005) Finite volume method for simulation of extrusion processes. Int J Numer Methods Eng 62(4):475–494
3. Belytschko T, Krongauz Y, Organ D, Fleming M, Krysl P (1996) Meshless methods: an overview and recent developments. Comput Methods Appl Mech Eng 139(1–4):3–47
4. Bohdal Ł, Tandecka K, Kałduński P (2017) Numerical simulation of shear slitting process of grain oriented silicon steel using SPH method. Acta Mech Autom 11(4):333–338
5. Campbell J (2003) Castings, 2nd edn. Elsevier, Amsterdam
6. Cleary PW, Ha J (2000) Three dimensional modelling of high pressure die casting. Int J Cast Metal Res 12(6):357–365
7. Cleary PW, Ha J (2002) Three-dimensional smoothed particle hydrodynamics simulation of high pressure die casting of light metal components. J Light Met 2(3):169–183
8. Cleary PW, Ha J, Nguyen T (2006) 3D SPH flow predictions and validation for high pressure die casting of automotive components. Appl Math Model 30(11):1406–1427
9. Cleary PW, Ha J, Prakash M, Nguyen T (2010) Short shots and industrial case studies: understanding fluid flow and solidification in high pressure die casting. Appl Math Model 34(8):2018–2033
10. Cleary PW, Savage G, Ha J, Prakash M (2014) Flow analysis and validation of numerical modelling for a thin walled high pressure die casting using SPH. Comput Part Mech 1(3):229–243
11. Fang J, Parriaux A (2008) A regularized Lagrangian finite point method for the simulation of incompressible viscous flows. J Comput Phys 227(20):8894–8908
12. Gavete L, Benito JJ, Ureña F (2016) Generalized finite differences for solving 3d elliptic and parabolic equations. Appl Math Model 40(2):955–965
13. Gimenez JM, Ramajo DE, Damián SM, Nigro NM, Idelsohn SR (2017) An assessment of the potential of PFEM-2 for solving long real-time industrial applications. Comput Part Mech 4(3):251–267
14. Jefferies A, Kuhnert J, Aschenbrenner L, Giffhorn U (2015) Finite pointset method for the simulation of a vehicle travelling through a body of water. In: Griebel M, Schweitzer MA (eds) Meshfree methods for partial differential equations VII, vol 100. Lecture notes in computational science and engineering. Springer, Berlin, pp 205–221
15. Kermanpur A, Mahmoudi S, Hajipour A (2008) Numerical simulation of metal flow and solidification in the multi-cavity casting moulds of automotive components. J Mater Process Technol 206(1–3):62–68
16. Kimatsuka A, Ohnaka I, Zhu JD, Ohmichi T (2003) Mold filling simulation with consideration of gas escape through sand mold. Int J Cast Metal Res 15(3):149–152
17. Koh CG, Gao M, Luo C (2012) A new particle method for simulation of incompressible free surface flow problems. Int J Numer Methods Eng 89(12):1582–1604
18. Kuhnert J (1999) General smoothed particle hydrodynamics. Ph.D. thesis, Technische Universität Kaiserslautern
19. Lewis RW, Ravindran K (2000) Finite element simulation of metal casting. Int J Numer Methods Eng 47(1–3):29–59
20. Liu GR (2009) Mesh free methods: moving beyond the finite element method, 2nd edn. CRC Press, Boca Raton
21. López YR, Roose D, Morfa CR (2013) Dynamic particle refinement in sPH: application to free surface flow and non-cohesive soil simulations. Comput Mech 51(5):731–741
22. Mirbagheri SMH, Esmaeileian H, Serajzadeh S, Varahram N, Davami P (2003) Simulation of melt flow in coated mould cavity in the casting process. J Mater Process Technol 142(2):493–507
23. Narowski P, Wilczynski K (2016) Simulation of polymer injection molding: a new practical approach to improve computation accuracy. Chall Mod Technol 7(3):25–28
24. Nguyen VP, Rabczuk T, Bordas S, Duflot M (2008) Meshless methods: a review and computer implementation aspects. Math Comput Simul 79(3):763–813
25. Park JS, Kim SM, Kim MS, Lee WI (2005) Finite element analysis of flow and heat transfer with moving free surface using fixed grid system. Int J Comput Fluid Dyn 19(3):263–276
26. Prohl A (1997) Projection and quasi-compressibility methods for solving the incompressible Navier–Stokes equations. Advances in numerical mathematics, 1st Edn. Vieweg + Teubner Verlag. https://doi.org/10.1007/978-3-663-11171-9
27. Quinlan NJ, Lobovskỳ L (2018) The finite volume particle method: toward a meshless technique for biomedical fluid dynamics. In:

Cerrolaza M, Shefelbine S, Garzón-Alvarado D (eds) Numerical methods and advanced simulation in biomechanics and biological processes. Academic Press, London, pp 341–354
28. Quinlan NJ, Lobovskỳ l, Nestor RM (2014) Development of the meshless finite volume particle method with exact and efficient calculation of interparticle area. Comput Phys Commun 185(6):1554–1563
29. Rao TVR (2007) Metal casting: principles and practice, 1st edn. New Age International, New Delhi
30. Ren J, Ouyang J, Jiang T, Li Q (2011) Simulation of complex filling process based on the generalized Newtonian fuid model using a corrected SPH scheme. Comput Mech 49:643–665
31. Reséndiz-Flores EO, Saucedo-Zendejo FR (2018) Meshfree numerical simulation of free surface thermal flows in mould filling processes using the finite pointset method. Int J Therm Sci 127:29–40
32. Reséndiz-Flores EO, Kuhnert J, Saucedo-Zendejo FR (2018) Application of a generalized finite difference method to mould filling process. Eur J Appl Math 29(3):450–469
33. Salinas C, Vasco DA, Moraga NO (2013) Two-dimensional non-Newtonian injection molding with a new control volume FEM/volume of fluid method. Int J Numer Methods Fluids 71(12):1509–1523
34. Saucedo-Zendejo FR, Reséndiz-Flores EO (2017) A new approach for the numerical simulation of free surface incompressible flows using a meshfree method. Comput Method Appl Mech Eng 324:619–639
35. Schmid M, Klein F (1995) Fluid flow in die cavities-experimental and numerical simulation, NADCA 18. In: International die casting congress and exposition, pp 93–99
36. Shadloo MS, Oger G, Touzé DL (2016) Smoothed particle hydrodynamics method for fluid flows, towards industrial applications: motivations, current state, and challenges. Comput Fluids 136:11–34
37. Sigalotti LDG, Klapp J, Rendón O, Vargas CA, Peña-Polo F (2016) On the kernel and particle consistency in smoothed particle hydrodynamics. Appl Numer Math 108:242–255
38. Szucki M, Suchy JS, Lelito J, Malinowski P, Sobczyk J (2017) Application of the lattice Boltzmann method for simulation of the mold filling process in the casting industry. Heat Mass Transf 53(12):3421–3431
39. Tiwari S, Kuhnert J (2001) Grid free method for solving the Poisson equation. Berichte des Fraunhofer ITWM 25
40. Tiwari S, Kuhnert J (2002) A meshfree method for incompressible fluid flows with incorporated surface tension. Revue Europeenne des Elements 11(7–8):965–987
41. Tiwari S, Kuhnert J (2003) Particle method for simulation of free surface flows. In: Hou Y, Tadmor E (eds) Hyperbolic problems: theory, numerics, applications. Springer, Berlin, pp 889–898
42. Tiwari S, Kuhnert J (2007) Modeling of two-phase flows with surface tension by finite pointset method (FPM). J Comput Appl Math 203(2):376–386
43. Xu X, Yu P (2017) Modeling and simulation of injection molding process of polymer melt by a robust SPH method. Appl Math Model 48:384–409